Universality of entanglement transitions from stroboscopic to continuous measurements

M. Szyniszewski*

Department of Physics, Lancaster University, Lancaster LA1 4YB, United Kingdom and
Department of Physics and Astronomy, University College London, London WC1E 6BT, United Kingdom

A. Romito and H. Schomerus

Department of Physics, Lancaster University, Lancaster LA1 4YB, United Kingdom

Measurement-driven transitions between extensive and sub-extensive scaling of the entanglement entropy receive interest as they illuminate the intricate physics of thermalization and control in open interacting quantum systems. Whilst this transition is well established for stroboscopic measurements in random quantum circuits, a crucial link to physical settings is its extension to continuous observations, where for an integrable model it has been shown that the transition changes its nature and becomes immediate. Here, we demonstrate that the entanglement transition at finite coupling persists if the continuously measured system is randomly nonintegrable, and show that it is smoothly connected to the transition in the stroboscopic models. This provides a bridge between a wide range of experimental settings and the wealth of knowledge accumulated for the latter systems.

Subjecting a complex quantum system to observations can have drastic effects on its time evolution. The most celebrated example is the quantum Zeno effect [1–3], according to which *continuous* projective measurements can freeze the dynamics of a quantum system completely. Recent work has established [4–8] and developed [9–39] an illuminating extension of this effect, where the quantum dynamics change in a phase transition when *stroboscopic* measurements occur with sufficient strength or frequency. This transition is manifested in the entanglement characteristics of the system, as captured by the entanglement entropy

$$S = \operatorname{tr}\left(\rho_A \ln \rho_A\right) \tag{1}$$

with the reduced density matrix of a subsystem A. In the transition, the entropy changes its scaling with the system size [5, 40–45] from extensive, indicating ergodic many-body dynamics, to sub-extensive, signaling localization of the underlying quantum-coherent correlations.

A key question to make this rapidly growing body of knowledge on stroboscopic systems applicable to physical settings is the fate of the entanglement transition for continuous variable-strength observations. These not only more accurately reflect the reality of many experimental architectures [46–55], but also enable to apply this knowledge to the generic effects of coupling to an environment that may not per se have been designed to carry out a measurement. For an integrable system, it has been shown that the transition can indeed completely change its nature when observations become continuous, in that it then can occur at infinitesimal small measurement strengths [56].

Here, we show that the transition from the stroboscopic models is reinstated for continuous observations of a randomly evolving, nonintegrable, system. We achieve this by formulating a model that allows us to interpolate between a stroboscopic random circuit and a continu-

ously evolving one, and trace the entanglement characteristics numerically in terms of the entanglement entropy and mutual information. The established link between these limits lends further relevance to deep results arrived for the stroboscopic circuits—such as emerging conformal symmetry [6, 7, 9–11] as well as approximations that permit to reach very large system sizes [4, 5, 7, 31–34, 57, 58]—giving them direct bearing on a much wider range of experimental settings.

Model.—We base our modeling on the universal quantum-circuit architecture [5, 59–61] shown in Fig. 1, which describes the dynamics of L spins (dots) evolving under the action of unitary gates U (rectangles) and nonunitary measurement operations M (diamonds) on individual spins. Two layers of gates and measurements make up one time step, dt, and iteration over n steps induces a discrete time evolution of the quantum state $|\psi_n\rangle$. In the original design [4–6], the gates are completely ran-
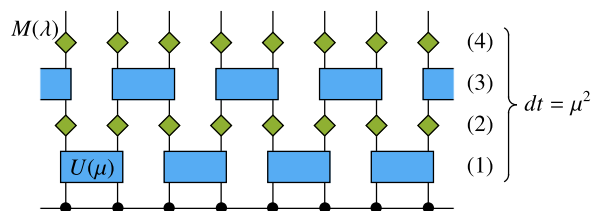

Figure 1. We study the entanglement dynamics in a random circuit model, combining unitary evolutions U and measurements M such that one can interpolate between the continuum limit (U near the identity matrix and measurements weak) and widely studied fully random, stroboscopic models. This is achieved by equipping the unitary matrices with a parameter μ that determines the physical time scale of the dynamics according to $dt \sim \mu^2$, and the measurements with a parameter λ so that the effective measurement strength is given by $\lambda_0 = \lambda/\mu$.

dom, according to unitary matrices U drawn from a circular ensemble with probability distribution given by the corresponding Haar measure, whilst the measurements are projective, so that the time step $dt = O(1)$ in terms of physical times scales governing the dynamics. This design can be easily adapted to other situations, including systems with deterministic dynamics [24–28, 36, 56] or other types of measurements [8, 11, 22, 23, 28, 36].

Here, we carry out two such modifications designed to change the dynamics and observation strength over the time scale dt, thereby allowing us to take the continuum limit in which $dt \to 0$.

(A) The unitary matrices U are generated from an ensemble parameterized by $0 \le \mu \le 1$, which interpolates between matrices close to the identity matrix ($\mu \ll 1$) and the exact Haar measure ($\mu = 1$). This is realized using the Poisson kernel [62],

$$U = (V + \sqrt{1 - \mu^2}\,\mathbb{1})(\mathbb{1} + \sqrt{1 - \mu^2}\,V)^{-1}, \qquad (2)$$

where V is a random unitary matrix distributed according to the Haar measure. The latter is recovered for $\mu = 1$, where $U = V$. For $\mu \ll 1$, the matrices localize close to the identity matrix,

$$U \approx \mathbb{1} - i\,dt\,H_{\text{eff}}, \quad dt \equiv \mu^2, \quad H_{\text{eff}} = \frac{i}{2}(V - \mathbb{1})(V + \mathbb{1})^{-1}, \qquad (3)$$

which identifies the Cayley transform of V as the effective Hamiltonian H_{eff}, and sets the physical time scale according to the resulting stable Cauchy process [63]. However, this Wiener process does not permit the exact extrapolation to the stroboscopic case. Between these limits, the matrices preserve unitarity and maintain randomness according to a probabilistic maximal-entropy principle [64, 65].

(B) The projective measurements are replaced by weak measurements, implemented by coupling the z-component of a given spin to an external pointer with a continuous readout x, prepared initially in a Gaussian state. Measurements are of strength λ, ranging from the case of no measurements ($\lambda = 0$) to the standard case of projective measurements ($\lambda \to \infty$). These take the form of positive-operator-value measurements [66, 67] with Kraus operators

$$M(x) = G(x - \lambda)\Pi_i^+ + G(x + \lambda)\Pi_i^-, \qquad (4)$$

where $G(x) = \exp(-x^2/2)/\pi^{1/4}$ is a Gaussian of unit width centered around zero, and $\Pi_i^\pm = (1 \pm \sigma^z)_i/2$ are projection operators onto spin-up or spin-down on site i. For a given readout x, the system state is updated via

$$|\psi\rangle \to \frac{1}{\sqrt{P(x)}} M(x)|\psi\rangle, \qquad (5)$$

where $P(x) = \langle\psi|M(x)^\dagger M(x)|\psi\rangle$ is the probability distribution of the measurement output. For small λ, the
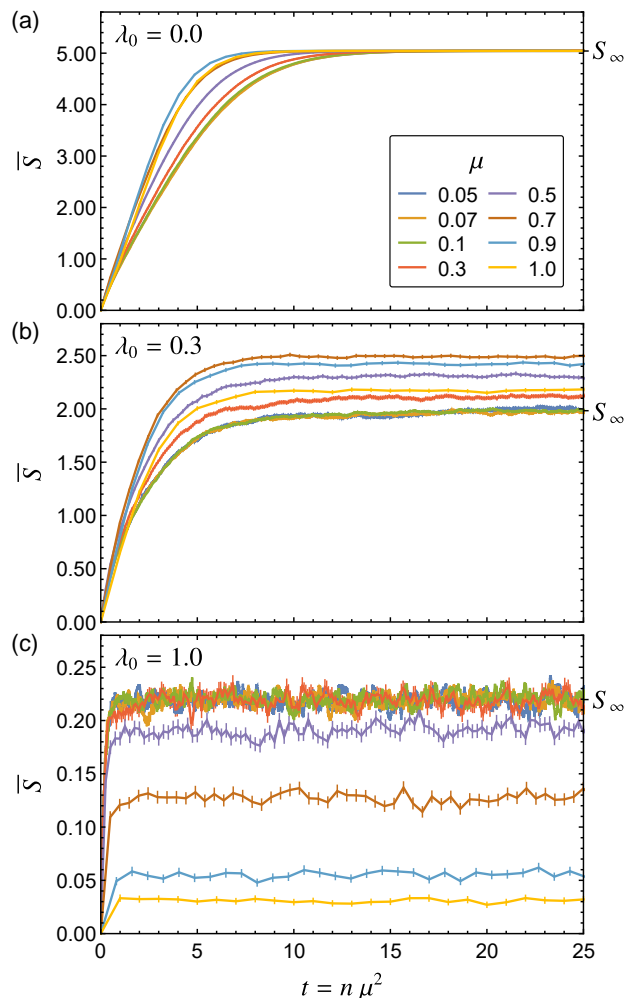

Figure 2. Entanglement dynamics in the random-circuit model of Fig. 1, as captured by the time evolution of the averaged bipartite entanglement entropy $\overline{S}$. Time is measured in units $t = n\mu^2$, the system size is $L = 16$, and results are averaged over 1000 realizations. The different panels fix the effective measurement strength to (a) $\lambda_0 = 0$, (b) $\lambda_0 = 0.3$, and (c) $\lambda_0 = 1.0$, with the different curves corresponding to different choices of μ. Throughout the whole dynamics, the curves collapse for $\mu \lesssim 0.1$, which indicates entering the continuum regime. Increasing the measurement strength suppresses the quasistationary value S_∞, which raises the question of an entanglement transition addressed in the subsequent figures.

measurement model reduces to a generic Wiener process

$$|\psi\rangle \to \mathcal{N}\left[1 - \sum_i \left(\lambda^2\langle\sigma_i^z\rangle + \delta W_i\right)\sigma_i^z\right]|\psi\rangle, \qquad (6)$$

where the random variables W_i are independently Gaussian-distributed with zero mean and variance λ^2, and $\mathcal{N}$ is a normalization constant.

Writing the intrinsic scale of this process as $\lambda^2 = \lambda_0^2\,dt = \lambda_0^2\mu^2$, the effective strength of the measurement

in our model is therefore given by

$$\lambda_0 = \lambda/\mu, \qquad (7)$$

which has to be kept fixed as we send $dt = \mu^2 \to 0$. The physical time scale for the dynamics is then given by $t = n\,dt = n\,\mu^2$, where n is the number of steps through the circuit depicted in Fig. 1. Our main result will be to establish that an entanglement transition occurs at a finite value of λ_0, for all scenarios from the continuum limit to the fully random stroboscopic case.

Entanglement dynamics in the continuum limit.— Figure 2 illustrates the effect of the described modifications on the entanglement dynamics in terms of the entanglement entropy for a subsystem of size $L/2$, averaged over 1000 realizations of the dynamics initialized to a Néel state. Time is measured as $t = n\mu^2$; in each panel, $\lambda_0 = \lambda/\mu$ is kept fixed, whilst each curve corresponds to a different value of μ.

In all cases, the entanglement entropy initially increases with time, but then saturates in a quasi-stationary regime, at a measurement-strength dependent value S_∞ that we will analyze further in the pursuit of the entanglement transition. For the moment, the key point in the figure is the collapse of curves at $\mu \lesssim 0.1$, which therefore delineates the continuum regime. That this collapse occurs both for the rate of entanglement spreading as well as for the saturation value confirms the described scaling of time and measurement strength in this regime. Outside of the continuum regime, the entanglement dynamics display a notable dependence on μ, both in the rate of initial entanglement spreading as well as for the saturation value, aspects to which we return later when we discuss the connection to the stroboscopic case. First, we establish that an entanglement transition occurs in the continuum regime, for which we set $\mu = 0.05$ (equivalently, $dt = 0.0025$).

This is demonstrated in Fig. 3, which shows the average and variance of the saturation value S_∞ of the entanglement entropy for different system sizes L as a function of the measurement strength λ_0. As seen in panel (a), the entanglement entropy is large and increases with system size when the measurement strength is small, but drops to a small, system-size-independent value when the measurement strength is large. As further illustrated in the inset, this qualitative change of the scaling occurs in the range $0.2 < \lambda_0 < 0.4$. Panel (b) shows that the sample-to-sample fluctuations var S_∞ indeed become large in this range. Whilst the position $\lambda_0^{\max}$ where the fluctuations are maximal drifts to smaller values as L is increased, its extrapolation to infinite system size (inset) yields a finite critical value $\lambda_0^{\mathrm{crit}} \approx 0.243(4)$. Using this critical value for finite-size scaling yields the critical exponent of the correlation length $\nu = 0.70(1)$ [68]. Panel (c) provides further evidence for the transition in terms of the tri-
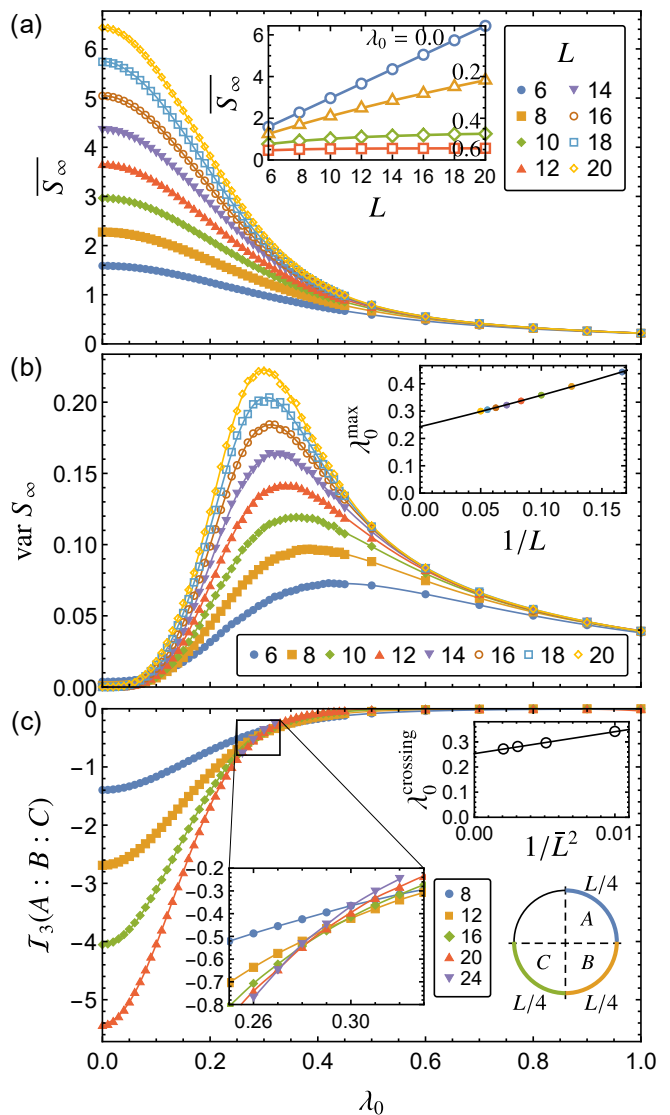

Figure 3. (a) Average saturation entropy $\overline{S_\infty}$ and (b) corresponding fluctuations var S_∞, as a function of measurement strength λ_0 for different system sizes L. The inset in (a) shows $\overline{S_\infty}$ for fixed λ_0 as L is increased, whilst the inset (b) shows the extrapolation of the position $\lambda_0^{\max}$ of maximal variance to an infinite system size. (c) Tripartite mutual information $\mathcal{I}_3(A : B : C)$ as a function of measurement strength λ_0 for different system sizes L, where the subsystems are all of size $L/4$, as indicated in the bottom right inset. The left inset focuses on the region where the curves cross, while the top right inset shows the extrapolation of the crossing positions to an infinite system size, where $\bar{L}$ is the average of the system sizes for which the crossing occurs.

partite mutual information

$$\mathcal{I}_3(A : B : C) = S(A) + S(B) + S(C) + S(A \cup B \cup C) \\ - S(A \cup B) - S(A \cup C) - S(B \cup C), \quad (8)$$

defined for three such subsystems A, B, and C. Here, the transition is indicated by the crossing point, which
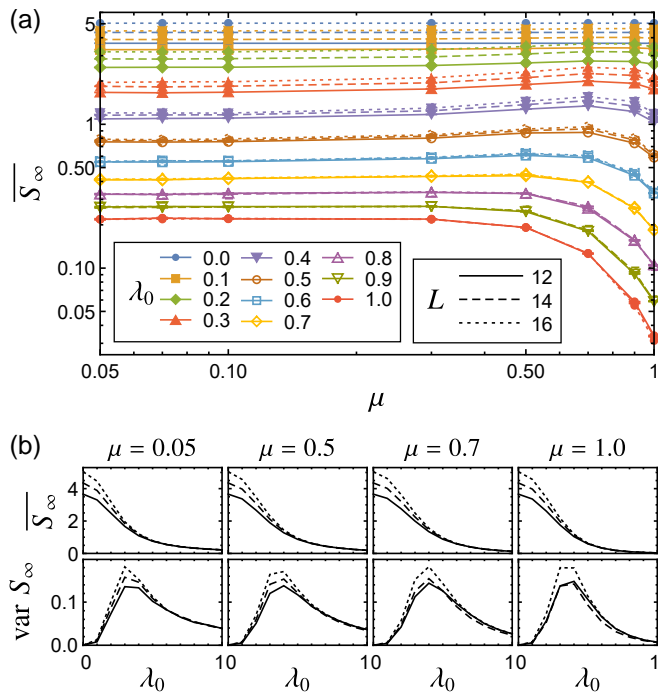
Figure 4. (a) Averaged saturation value $\overline{S_\infty}$ of the entanglement entropy for different values of μ in the whole range from the continuum limit ($\mu \to 0$) to the fully random stroboscopic case ($\mu = 1$). In each curve, the measurement strength $\lambda_0 = \lambda/\mu$ and the system size are kept fixed. Across the whole range of μ, the entanglement entropy changes its scaling from extensive to subextensive around $\lambda_0 \approx 0.3$. As shown in the subpanels in (b), the qualitative entanglement characteristics in the continuum regime [Fig. 3(a) and (b)] indeed also occur for intermediate values ($\mu = 0.5$ and $\mu = 0.7$), with $\mu = 1$ reproducing the conventional stroboscopic case.

has been found to show reduced finite-size effects in the original stroboscopic model [17]. As shown in the insets, these features also hold in the present model, with the position of the crossings approaching a critical value of $\lambda_0^{\mathrm{crit}} = 0.253(2)$ that agrees well with the transition point obtained using the variance analysis [68].

Connection to the stroboscopic case.—Having established the entanglement transition in the continuum regime, we now come to the second main point of this paper, namely, its connection to the transition in the original stroboscopic model. This is afforded in our model by being able to tune the timescale $dt = \mu^2$ from 0 to 1. Returning to Fig. 2, outside the continuum regime the measurements still have the effect to suppress the saturation entropy, but down to even smaller, μ-dependent, values. For a detailed analysis, Figure 4 (a) shows how the saturation entanglement entropy changes with μ for fixed λ_0, where differently-articulated curves correspond to different system sizes L. Depending on the measurement strength, we find two scenarios. For $\lambda_0 \lesssim 0.4$, the saturation entropy remains essentially μ-independent, and shows a systematic system-size dependence with an ex-

tensive scaling, corresponding to ergodic behavior. For larger measurement strengths, on the other hand, the entropy displays the above-mentioned downturn as one approaches the stroboscopic limit—but also becomes independent of the system size across the whole parameter range. As shown in the subpanels in (b), in the intermediate range between the continuum regime and the stroboscopic case, the average and fluctuations of the entanglement entropy display the same qualitative behavior as in Fig. 3, with an only weak μ dependence of the critical value $\lambda_0^{\mathrm{crit}}$. These results demonstrate a substantial degree of universality of the entanglement transition in the whole range from the continuum regime to the fully random stroboscopic case.

Conclusions.—In summary, we showed that measurement-driven entanglement transitions can occur in continuously evolving and monitored systems. We established this in a flexible extension of random-circuit models, by which we could directly related the transition to the widely studied stroboscopic case. This uncovered a significant degree of university in the entanglement dynamics. As we show in Ref. [68], this universality further extends to the variation of the measurement frequency p (the parameter that was varied in the original studies of the stroboscopic model), where results remain invariant upon a simple rescaling $\lambda_0 = \sqrt{p}\lambda/\mu$ of the effective measurement strength. In this way, results derived for stroboscopic models gain a much larger range of applicability.

The model described in this work has been designed to not only interpolate between different scenarios, but also to combine the most generic effects of random dynamics and continuous measurements, and thereby, to further inform the design of suitable experiments. In particular, the unitary dynamics describe the local generation of entanglement by randomly fluctuating interactions, whilst the employed measurement model describes quantum detection schemes currently employed in solid state nanocircuits [49, 51, 69–71] and quantum optical devices [72, 73]. In such settings, the described universality of the entanglement dynamics enhances our understanding of environmental effects, and serves to provide detailed control of the quantum dynamics in simple yet profound ways.

APPENDIX A: FURTHER ENTANGLEMENT CHARACTERISTICS

Figure 5 presents our data for the bipartite mutual information

$$\mathcal{I}_2(A:B) = S(A) + S(B) - S(A \cup B). \qquad (9)$$

This is defined for two subsystems A and B, here chosen to be antipodal, whose size is varied proportionally to the overall system size in the ratio of (a) $1/4$, (b) $1/6$, and (c) $1/8$. Whilst each case provides characteristic maxima and crossings in the range $0.2 \lesssim \lambda_0 \lesssim 0.4$, these occur at different locations and show inconsistent finite-size effects, making this quantity less suitable to determine the transition when compared to the bipartite entropy and tripartite mutual information studied in the main text.

We also note that the Hartley entropy $[(n = 0)$-Rényi entropy], which for projective measurements exhibits a phase transition at a different critical frequency p_c than other Rényi entropies [6, 17], in our model is always maximal for any $\lambda_0 < \infty$, as the weak measurements never completely break bonds in the circuit.
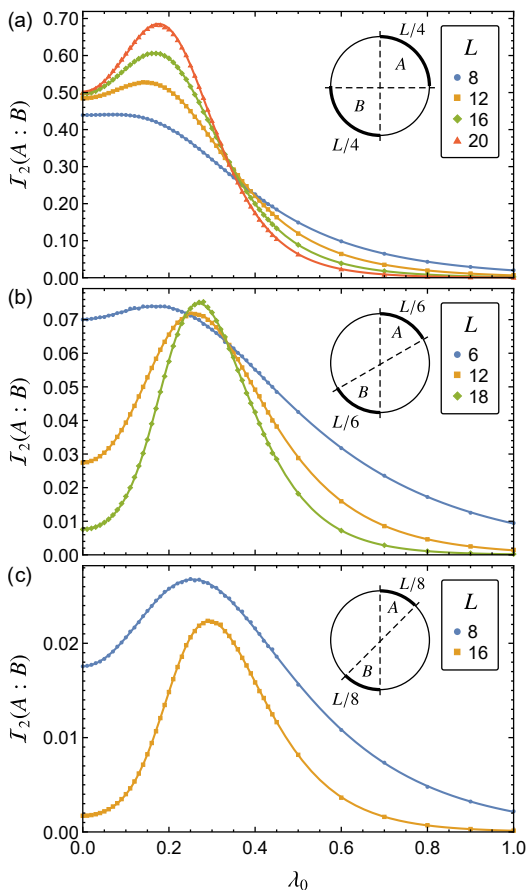

Figure 5. Bipartite mutual information $\mathcal{I}_2(A : B)$ for antipodal subsystems of size (a) $L/4$, (b) $L/6$, and (c) $L/8$.
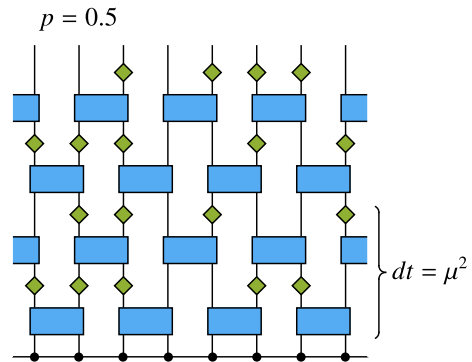

Figure 6. Illustration of a random circuit with measurement frequency $p = 1/2$. In the continuum limit, this results in the same behavior as the original circuit with altered effective measurement strength $\lambda_0^{\mathrm{eff}} = \sqrt{p}\lambda/\mu$.

APPENDIX B: MEASUREMENT FREQUENCY

In this Appendix, we address the issue of applying the measurements M with a specific frequency $p \in [0, 1]$, a question that has been explored in many recent studies in the original stroboscopic model [4–8]. For illustration, a modified circuit with $p = 1/2$ is shown in Fig. 6.

As shown in Fig. 7, the entanglement characteristics of the system remain invariant for a constant value of

$$\lambda_0^{\mathrm{eff}} = \sqrt{p}\lambda/\mu, \qquad (10)$$

which becomes exact in the continuum limit, and is this key feature mentioned in the conclusions. For completeness, we show in Fig. 8 that the entanglement characteristics from our model in the continuum limit, panel (a), are qualitatively the same as obtained in the stroboscopic case with variable-strength measurements (b) or projective measurements with rate p (c), where parameters are rescaled in analogy to Eq. (10).

APPENDIX C: EXTRAPOLATION TO THE INFINITE SYSTEM SIZE

This Appendix details the fitting procedures used to extract the infinite-system-size values in Fig. 3. Both λ_0^{max} and $\lambda_0^{\mathrm{crossing}}$ have an unknown dependence on the system size. We, therefore, used a standard polynomial fitting procedure in $1/L$.

By analyzing the fits for λ_0^{max} with polynomial forms up to the first, the second and the third order in $1/L$, we have determined that the linear fit underfits the data, while the fit with terms up to $1/L^3$ overfits the data. The quadratic fit was found to match the data best. We note that the polynomial expansion of λ_0^{max} in $1/L$ is also motivated by previous numerical results in Ref. [8] (circuit with stroboscopic weak measurements), where λ^{max} was found to be a polynomial function of $1/L$, while p^{max} – a
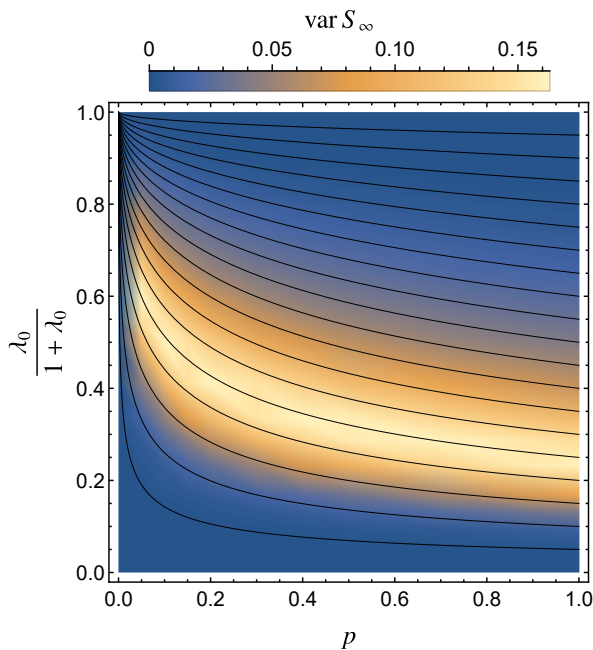
Figure 7. Contour plot of the variance $\operatorname{var} S_\infty$ of the saturation entropy as a function of measurement frequency p and the (not rescaled) measurement strength $\lambda_0 = \lambda/\mu$, for system size $L = 14$. The black lines show contours of equivalent systems with fixed $\lambda_0^{\text{eff}} = \sqrt{p}\lambda_0$.

polynomial function of $1/L^2$. This is consistent with our discussions in Appendix B, where we show that λ_0 from the continuum limit behaves like λ in the stroboscopic limit with $p = 1$, and furthermore scales with $\sqrt{p}$ in the stroboscopic limit with $\lambda \to \infty$.

A similar analysis for $\lambda_0^{\text{crossing}}$ reveals that the linear contribution in $1/L$ is statistically irrelevant. We therefore adopted a polynomial fit in $1/L^2$, and after similar investigation as above, a linear fit was found to describe the data best, while quadratic fit in $1/L^2$ was overfitting our data.

APPENDIX D: FINITE SIZE SCALING OF THE ENTANGLEMENT ENTROPY

In order to extract the critical exponent of ν of the correlation length, we attempted finite size scaling of the entanglement entropy, using the following scaling ansatz proposed in Ref. [6]:

$$|\overline{S_\infty}(\lambda_0) - \overline{S_\infty}(\lambda_0^{\text{crit}})| = F\left[(\lambda_0 - \lambda_0^{\text{crit}})L^{1/\nu}\right], \quad (11)$$

where F is an unknown one-parameter scaling function. Assuming $\lambda_0^{\text{crit}} = 0.243$ extracted from the variance analysis (see the main text), the data collapse [shown in Fig. 9(a)] gives $\nu = 0.70(1)$. The same scaling for the stroboscopic limit [8] with $\lambda_0 = 0.301$ yields $\nu = 0.80(3)$ [see Fig. 9(b)]. The two estimates of ν are close, and

since we do not account for all finite size errors, it may be that both critical exponents agree.

APPENDIX E: COMPARISON BETWEEN THE CAUCHY PROCESS AND WIENER PROCESS

In the main text, we approach the limit of continuous stochastic quantum dynamics based on a Cauchy process, which allows us to interpolate between this limit and the stroboscopic case with random unitaries distributed by the Haar measure. In order to assert that the results from this process are generic, we compare these in this Appendix to those of a Wiener process. This Wiener process is realized by replacing H_{eff} in Eq. (3) by an $N \times N$-dimensional Hermitian matrix with Gaussian-distributed elements with $\langle |H_{\text{eff},lm}|^2 \rangle = \sigma^2/dt$, where $N = 4$ for dynamics generated by acting onto two spins. Therefore, in the Wiener process matrix elements have to be scaled as $H_{\text{eff},lm} \sim \mu^{-1}$, which is as expected given that $\mu^{-1} = dt^{-1/2}$. Indeed, the processes can be related by comparing the ensemble averages of the resulting unitary matrices, for which we find

$$\langle |U_{nn}|^2 \rangle = \begin{cases} 1 - dt(N-1)\sigma^2 & \text{(Wiener)}; \\ 1 - dt(N-1)/(N+1) & \text{(Cauchy)}; \end{cases}$$
$$(12)$$

$$\langle |U_{n \neq m}|^2 \rangle = \begin{cases} dt\,\sigma^2 & \text{(Wiener)}; \\ dt/(N+1) & \text{(Cauchy)}. \end{cases} \quad (13)$$

(for the Cauchy process we adopted results from [74]).

We confirmed this scaling numerically by matching the transient dynamical entanglement growth rate in both processes, which we found to agree with a fixed proportionality constant that is independent of the overall system size and other parameters of the model. As shown in Fig. 10, using this input from the transient dynamics, we furthermore find exactly the same dependence of the averaged entropy and mutual information in both processes. Finally, the fluctuations of the entropy, which further probe details of the temporal correlations, match when rescaled by a multiplicative factor of order of unity, which is again the same for all parameters and system sizes. These observations further support the universal character of the entanglement transition, which displays the same generic behavior across all described scenarios.

----

* mszynisz@gmail.com

[1] A. Degasperis, L. Fonda, and G. C. Ghirardi, Does the lifetime of an unstable system depend on the measuring apparatus?, Nuov. Cim. A **21**, 471 (1974).
[2] B. Misra and E. C. G. Sudarshan, The Zeno's paradox in quantum theory, J. Math. Phys. **18**, 756 (1977).
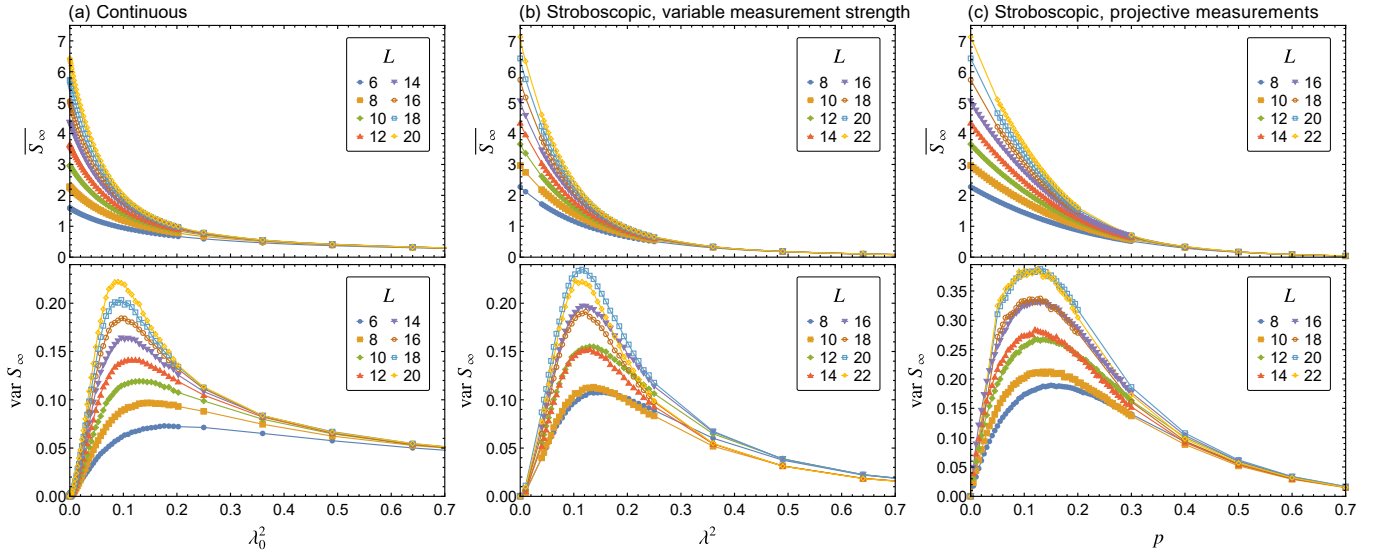[3] A. Peres, Zeno paradox in quantum theory, Am. J. Phys. **48**, 931 (1980).

Figure 8. Comparison of the entanglement characteristics from (a) the model of the main text in the continuum limit ($\mu, \lambda \ll 1$ at fixed $\lambda_0 = \lambda/\mu$) as well as the stroboscopic case ($\mu = 1$) with (b) measurements of variable strength λ or (c) projective measurements with rate p.
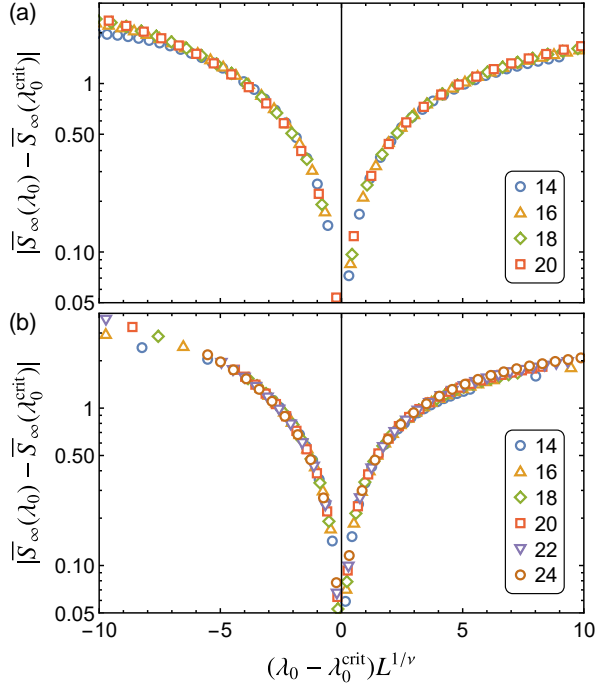

Figure 9. Finite size scaling of the saturation entanglement entropy using the scaling from Eq. (11) for (a) the continuum limit ($\mu \to 0$) and (b) the stroboscopic model ($\mu = 1$).

[4] Y. Li, X. Chen, and M. P. A. Fisher, Quantum Zeno effect and the many-body entanglement transition, Phys. Rev. B **98**, 205136 (2018).

[5] A. Chan, R. M. Nandkishore, M. Pretko, and G. Smith, Unitary-projective entanglement dynamics, Phys. Rev. B **99**, 224307 (2019).

[6] B. Skinner, J. Ruhman, and A. Nahum, Measurement-induced phase transitions in the dynamics of entanglement, Phys. Rev. X **9**, 031009 (2019).

[7] Y. Li, X. Chen, and M. P. A. Fisher, Measurement-driven entanglement transition in hybrid quantum circuits, Phys. Rev. B **100**, 134306 (2019).

[8] M. Szyniszewski, A. Romito, and H. Schomerus, Entanglement transition from variable-strength weak measurements, Phys. Rev. B **100**, 064204 (2019).

[9] C.-M. Jian, Y.-Z. You, R. Vasseur, and A. W. W. Ludwig, Measurement-induced criticality in random quantum circuits, Phys. Rev. B **101**, 104302 (2020).

[10] Y. Li, X. Chen, A. W. W. Ludwig, and M. P. A. Fisher, Conformal invariance and quantum non-locality in hybrid quantum circuits, arXiv:2003.12721 (2020).

[11] X. Chen, Y. Li, M. P. A. Fisher, and A. Lucas, Emergent conformal symmetry in non-unitary random dynamics of free fermions, arXiv:2004.09577 (2020).

[12] S. Choi, Y. Bao, X.-L. Qi, and E. Altman, Quantum error correction in scrambling dynamics and measurement induced phase transition, arXiv:1903.05124 (2019).

[13] M. J. Gullans and D. A. Huse, Dynamical purification phase transitions induced by quantum measurements, arXiv:1905.05195 (2019).

[14] W.-T. Kuo, A. A. Akhtar, D. P. Arovas, and Y.-Z. You, Markovian entanglement dynamics under locally scrambled quantum evolution, arXiv:1910.11351 (2019).

[15] A. Nahum and B. Skinner, Entanglement and dynamics of diffusion-annihilation processes with Majorana defects, arXiv:1911.11169 (2019).

[16] S. Roy, J. T. Chalker, I. V. Gornyi, and Y. Gefen, Measurement-induced steering of quantum systems, arXiv:1912.04292 (2019).

[17] A. Zabalo, M. J. Gullans, J. H. Wilson, S. Gopalakrishnan, D. A. Huse, and J. H. Pixley, Critical properties of the measurement-induced transition in random quantum circuits, Phys. Rev. B **101**, 060301(R) (2020).
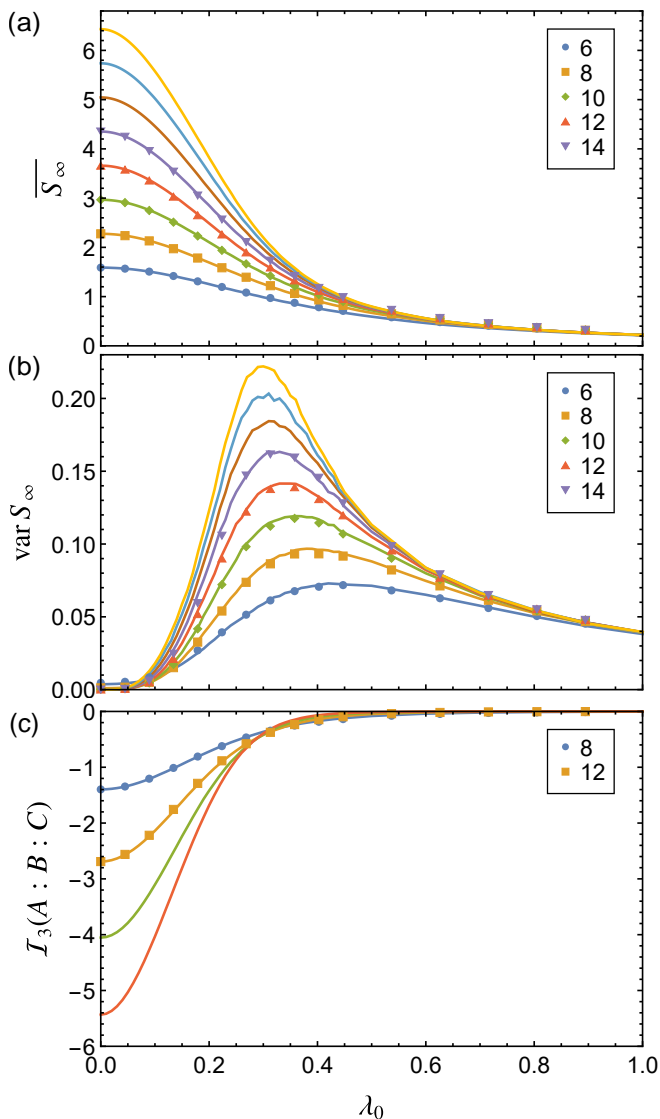
[18] L. Zhang, J. A. Reyes, S. Kourtis, C. Chamon, E. R.

Figure 10. Comparison between the Cauchy process (lines) and the Wiener process (markers) for (a) average saturation entropy $\overline{S_\infty}$, (b) corresponding fluctuations varS_∞, and (c) tripartite mutual information $\mathcal{I}_3(A : B : C)$. The size of the fluctuations for the Cauchy process was normalized to match the Wiener process.

Mucciolo, and A. E. Ruckenstein, Nonuniversal entanglement level statistics in projection-driven quantum circuits, arXiv:2001.11428 (2020).

[19] R. Fan, S. Vijay, A. Vishwanath, and Y.-Z. You, Self-organized error correction in random unitary circuits with measurement, arXiv:2002.12385 (2020).

[20] Y. Bao, S. Choi, and E. Altman, Theory of the phase transition in random unitary circuits with measurements, Phys. Rev. B **101**, 104301 (2020).

[21] A. Bera and S. S. Roy, Growth of genuine multipartite entanglement in random unitary circuits, arXiv:2003.12546 (2020).

[22] A. Lavasani, Y. Alavirad, and M. Barkeshli, Measurement-induced topological entanglement

[23] S. Sang and T. H. Hsieh, Measurement protected quantum phases, arXiv:2004.09509 (2020).

[24] M. Ippoliti, M. J. Gullans, S. Gopalakrishnan, D. A. Huse, and V. Khemani, Entanglement phase transitions in measurement-only dynamics, arXiv:2004.09560 (2020).

[25] Q. Tang and W. Zhu, Measurement-induced phase transition: A case study in the nonintegrable model by density-matrix renormalization group calculations, Phys. Rev. Research **2**, 013022 (2020).

[26] D. Rossini and E. Vicari, Measurement-induced dynamics of many-body systems at quantum criticality, arXiv:2001.11501 (2020).

[27] S. Goto and I. Danshita, Measurement-induced transitions of the entanglement scaling law in ultracold gases with controllable dissipation, arXiv:2001.03400 (2020).

[28] Y. Fuji and Y. Ashida, Measurement-induced quantum criticality under continuous monitoring, arXiv:2004.11957 (2020).

[29] K. Snizhko, P. Kumar, and A. Romito, The quantum Zeno effect appears in stages, arXiv:2003.10476 (2020).

[30] V. Gebhart, K. Snizhko, T. Wellens, A. Buchleitner, A. Romito, and Y. Gefen, Topological transition in measurement-induced geometric phases, PNAS **117**, 5706 (2020).

[31] M. J. Gullans and D. A. Huse, Scalable probes of measurement-induced criticality, arXiv:1910.00020 (2019).

[32] J. Lopez-Piqueres, B. Ware, and R. Vasseur, Mean-field theory of entanglement transitions from random tree tensor networks, arXiv:2003.01138 (2020).

[33] O. Shtanko, Y. A. Kharkov, L. P. García-Pintos, and A. V. Gorshkov, Classical models of entanglement in monitored random circuits, arXiv:2004.06736 (2020).

[34] K. Noh, L. Jiang, and B. Fefferman, Efficient classical simulation of noisy random quantum circuits in one dimension, arXiv:2003.13163 (2020).

[35] B.-L. Fang, J. Chen, F. Chen, and L. Ye, Weak measurement induced asymmetric quantum cloning, Laser Phys. Lett. **17**, 085203 (2020).

[36] O. Alberton, M. Buchhold, and S. Diehl, Trajectory dependent entanglement transition in a free fermion chain – from extended criticality to area law, arXiv:2005.09722 (2020).

[37] O. Lunt and A. Pal, Measurement-induced entanglement transitions in many-body localized systems, arXiv:2005.13603 (2020).

[38] X. Turkeshi, R. Fazio, and M. Dalmonte, Measurement-induced criticality in (2+1)-d hybrid quantum circuits, arXiv:2007.02970 (2020).

[39] Y. Li and M. P. A. Fisher, Statistical mechanics of quantum error-correcting codes, arXiv:2007.03822 (2020).

[40] M. Žnidarič, T. Prosen, and P. Prelovšek, Many-body localization in the Heisenberg XXZ magnet in a random field, Phys. Rev. B **77**, 064426 (2008).

[41] J. Eisert, M. Cramer, and M. B. Plenio, Colloquium: Area laws for the entanglement entropy, Rev. Mod. Phys. **82**, 277 (2010).

[42] J. H. Bardarson, F. Pollmann, and J. E. Moore, Unbounded growth of entanglement in models of many-body localization, Phys. Rev. Lett. **109**, 017202 (2012).

[43] B. Bauer and C. Nayak, Area laws in a many-body loc-

alized state and its implications for topological order, J. Stat. Mech. Theory Exp. **2013**, P09005 (2013).

[44] J. A. Kjäll, J. H. Bardarson, and F. Pollmann, Many-body localization in a disordered quantum Ising chain, Phys. Rev. Lett. **113**, 107204 (2014).

[45] D. J. Luitz, N. Laflorencie, and F. Alet, Many-body localization edge in the random-field Heisenberg chain, Phys. Rev. B **91**, 081103(R) (2015).

[46] J. R. Petta, A. C. Johnson, J. M. Taylor, E. A. Laird, A. Yacoby, M. D. Lukin, C. M. Marcus, M. P. Hanson, and A. C. Gossard, Coherent manipulation of coupled electron spins in semiconductor quantum dots, Science **309**, 2180 (2005).

[47] D. Kim, Z. Shi, C. Simmons, D. Ward, J. Prance, T. S. Koh, J. K. Gamble, D. Savage, M. Lagally, M. Friesen, *et al.*, Quantum control and process tomography of a semiconductor quantum dot hybrid qubit, Nature **511**, 70 (2014).

[48] A. West, B. Hensen, A. Jouan, T. Tanttu, C.-H. Yang, A. Rossi, M. F. Gonzalez-Zalba, F. Hudson, A. Morello, D. J. Reilly, *et al.*, Gate-based single-shot readout of spins in silicon, Nat. Nanotechnol. **14**, 437 (2019).

[49] K. Murch, S. Weber, C. Macklin, and I. Siddiqi, Observing single quantum trajectories of a superconducting quantum bit, Nature **502**, 211 (2013).

[50] P. Neumann, J. Beck, M. Steiner, F. Rempp, H. Fedder, P. R. Hemmer, J. Wrachtrup, and F. Jelezko, Single-shot readout of a single nuclear spin, Science **329**, 542 (2010).

[51] D. Aasen, M. Hell, R. V. Mishmash, A. Higginbotham, J. Danon, M. Leijnse, T. S. Jespersen, J. A. Folk, C. M. Marcus, K. Flensberg, and J. Alicea, Milestones toward Majorana-based quantum computing, Phys. Rev. X **6**, 031016 (2016).

[52] J. Manousakis, C. Wille, A. Altland, R. Egger, K. Flensberg, and F. Hassler, Weak measurement protocols for Majorana bound state identification, Phys. Rev. Lett. **124**, 096801 (2020).

[53] J. F. Steiner and F. von Oppen, Readout of Majorana qubits, arXiv:2004.02124 (2020).

[54] M. I. K. Munk, R. Egger, J. Schulenborg, and K. Flensberg, Parity-to-charge conversion in Majorana qubit readout, arXiv:2004.02123 (2020).

[55] P. Maioli, T. Meunier, S. Gleyzes, A. Auffeves, G. Nogues, M. Brune, J. M. Raimond, and S. Haroche, Nondestructive Rydberg atom counting with mesoscopic fields in a cavity, Phys. Rev. Lett. **94**, 113601 (2005).

[56] X. Cao, A. Tilloy, and A. D. Luca, Entanglement in a fermion chain under continuous monitoring, SciPost Phys. **7**, 24 (2019).

[57] J. Napp, R. L. L. Placa, A. M. Dalzell, F. G. S. L. Brandao, and A. W. Harrow, Efficient classical simulation of random shallow 2d quantum circuits, arXiv:2001.00021 (2019).

[58] T. Zhou and A. Nahum, The entanglement membrane in chaotic many-body systems, arXiv:1912.12311 (2019).

[59] A. Nahum, J. Ruhman, S. Vijay, and J. Haah, Quantum entanglement growth under random unitary dynamics, Phys. Rev. X **7**, 031016 (2017).

[60] C. W. von Keyserlingk, T. Rakovszky, F. Pollmann, and S. L. Sondhi, Operator hydrodynamics, OTOCs, and entanglement growth in systems without conservation laws, Phys. Rev. X **8**, 021013 (2018).

[61] A. Nahum, S. Vijay, and J. Haah, Operator spreading in random unitary circuits, Phys. Rev. X **8**, 021014 (2018).

[62] L. Hua, *Harmonic analysis of functions of several complex variables in the classical domains* (American Mathematical Society, Providence, R.I., 1963).

[63] The Cauchy process arises from the Lorentzian distribution of H_{eff}; see, e.g., Ref. [65]. An analogous entanglement dynamics can be obtained from a Wiener process where H_{eff} is taken from the Gaussian unitary ensemble with matrix elements $H_{\text{eff},lm} = O(1/\mu)$; for more details see [68].

[64] P. A. Mello, P. Pereyra, and T. H. Seligman, Information theory and statistical nuclear reactions. i. general theory and applications to few-channel problems, Ann. Phys. (N. Y.) **161**, 254 (1985).

[65] P. W. Brouwer, Generalized circular ensemble of scattering matrices for a chaotic cavity with nonideal leads, Phys. Rev. B **51**, 16878 (1995).

[66] K. Jacobs, *Quantum measurement theory and its applications* (Cambridge University Press, 2014).

[67] H. M. Wiseman and G. J. Milburn, *Quantum measurement and control* (Cambridge University Press, 2009).

[68] See the Supplemental Material for an analysis of the transition in terms of the bipartite information, a discussion of the role of measurement frequency, the description and further discussion of the finite-size scaling, and a comparison between different stochastic processes that can be used to approach the continuum limit. This Supplemental Material also includes a reference to Ref. [74].

[69] M. Field, C. G. Smith, M. Pepper, D. A. Ritchie, J. E. F. Frost, G. A. C. Jones, and D. G. Hasko, Measurements of Coulomb blockade with a noninvasive voltage probe, Phys. Rev. Lett. **70**, 1311 (1993).

[70] A. N. Korotkov, Continuous quantum measurement of a double dot, Phys. Rev. B **60**, 5737 (1999).

[71] A. Romito, Y. Gefen, and Y. M. Blanter, Weak values of electron spin in a double quantum dot, Phys. Rev. Lett. **100**, 056801 (2008).

[72] O. Hosten and P. Kwiat, Observation of the spin Hall effect of light via weak measurements, Science **319**, 787 (2008).

[73] P. B. Dixon, D. J. Starling, A. N. Jordan, and J. C. Howell, Ultrasensitive beam deflection measurement via interferometric weak value amplification, Phys. Rev. Lett. **102**, 173601 (2009).

[74] F. Haake, M. Kus, H.-J. Sommers, H. Schomerus, and K. Zyczkowski, Secular determinants of random unitary matrices, J. Phys. A **29**, 3641 (1996).